The Identification of MiRNA and MRNA Expression Profiles Associated with Pediatric Atypical Teratoid/rhabdoid Tumor

Xinke Xu
The First Affiliated Hospital of Jinan University
Hongyao Yuan
The First Affiliated Hospital of Jinan University
Junping Pan
The First Affiliated Hospital of Jinan University
Wei Chen
Guangzhou Women and Children's Medical Center
Cheng Chen
Guangzhou Women and Children's Medical Center
Yang Li
Guangzhou Women and Children's Medical Center
Fangcheng Li (sjwklfc@126.com)
The First Affiliated Hospital of Jinan University

Research Article

Keywords: Atypical teratoid, mRNA, microRNA, Expression profiles, Immunocyte infiltration

Posted Date: October 26th, 2021

DOI: https://doi.org/10.21203/rs.3.rs-986121/v1

Abstract

Background: Atypical teratoid/rhabdoid tumor (AT/RT) is a malignant pediatric tumor of the central nervous system (CNS) with high recurrence and low survival rates that is often misdiagnosed. MicroRNAs (miRNAs) are involved in the tumorigenesis of numerous pediatric cancers, but their roles in AT/RT remain unclear.

Methods: In this study, we used miRNA sequencing and gene expression microarrays from patient tissue to study both the miRNAome and transcriptome traits of AT/RT.

Results: Our findings demonstrate that 5 miRNAs were up-regulated, 16 miRNAs were down-regulated, 179 mRNAs were up-regulated and 402 mRNAs were down-regulated in AT/RT. The expressions of hsa-miR-17-5p and MAP7 mRNA showed the most significant differences in AT/RT tissues as assayed by qPCR, and analyses using the miRTarBase database identified MAP7 mRNA as a target gene of hsa-miR-17-5p.

Conclusions: Our findings suggest that the dysregulation of hsa-miR-17-5p may be a pivotal event in AT/RT and MAP7 miRNAs that may represent potential therapeutic targets and diagnostic biomarkers.

1. Background

Atypical teratoid/rhabdoid tumor (AT/RT) is the most common malignant embryonal central nervous system (CNS) tumor in children below 12 months of age and its incidence rate decreases with age thereafter [1, 2]. AT/RT was first identified as one of the embryo tumors that represent approximately 1–2% of pediatric intracranial tumors [3]. Because of the lack of clinical manifestation and radiography characteristics, the early clinical diagnosis of AT/RT remains challenging [4]. The treatment options for AT/RT currently include surgical resection, chemotherapy and radiotherapy [5–7]. However, the prognosis for pediatric patients with AT/RT is still dismal, with a median survival of 15.4 months. Studies have shown that the majority of AT/RT patients show genomic mutations in *SMARCB1* (also known as *INI1*) [8]. However, the precise pathogenesis of this disease is unclear. The identification of novel therapeutics based on the specific mechanism of AT/RT carcinogenesis is therefore critical.

Recent studies have shown that microRNAs (miRNAs) play a vital role in CNS tumorigenesis. MiRNAs, a subtype of small non-coding RNAs, regulate gene expression through recognizing and binding to seed sequence–matching sites in the 3' untranslated regions of target mRNAs [9–11]. MiRNAs are involved in the pathogenesis of human malignant tumors and function as oncogenes or tumor suppressors, depending on their downstream targets [12–14]. Previous studies have identified abnormal miRNA levels in patients with tumors in the CNS, indicating that miRNAs may play a key role in CNS tumor development [15]. However, knowledge of the miRNA expression profile of AT/RT patients is still limited.

In this study, we analyzed miRNA expression profiles of pediatric AT/RT tumors by analyzing public datasets GSE42656 and GSE42657. Our results revealed that 5 miRNAs were significantly upregulated

and 16 miRNAs were significantly downregulated in tumor tissue. Furthermore, Kyoto Encyclopedia of Genes and Genomes (KEGG) analysis was applied to evaluate the regulatory network for these differentially expressed miRNAs that may exert vital regulatory functions in the tumorigenesis of AT/RT. Our results suggest that abnormal miRNA expression may play key functions in the tumorigenesis in AT/RT and may represent potential targets for clinical treatment.

2. Methods

2.1 Differential expression analysis of GEO datasets

AT/RT expression datasets GSE42656 (https://www.ncbi.nlm.nih.gov/geo/query/acc.cgi?acc=GSE42656) and GSE42657 (https://www.ncbi.nlm.nih.gov/geo/query/acc.cgi?acc=GSE42657) were processed by edgeR package in RStudio (version 3.5.0), with a significant cutoff |log2FC|>2 and *P*-value <0.01 [16]. The gene expression profile GSE42656 contains eight control and five AT/RT patients. The miRNA expression dataset is derived from GSE42657, which includes seven control and five tumor tissues. Detailed information for the expression profiles are listed in Table 1.

2.2 Functional analysis

Based on the differential expression analysis, we identified the related signaling pathways using Gene Ontology (GO) enrichment analysis. GO terms have three different modules: biological process (BP), molecular function (MF), and cellular component (CC). KEGG pathway analysis was then used to identify the significant pathways for dysregulated mRNAs. GO and KEGG analysis were both used in cluster profiler package in R studio [17]. The *P*-value was calculated for each enriched function and/or pathway.

2.3 Immunocyte infiltration annotation

We used the CIBERSORT approach to identify inflammatory gene expression signatures in silico to identify the characteristics of the immune response in AT/RT. CIBERSORT is a computational framework for high-throughput characterization of immune cells [18].

2.4 miRNA-mRNA pair analysis

We used miRTarBase to predict the target genes of the differentially expressed miRNAs (http://mirtarbase.mbc.nctu.edu.tw/) [19]. Differentially Expressed Genes (DEGs) were extracted and the putative miRNA-mRNA regulatory network was constructed using Cytoscape software (version 3.7.0). To validate the miRNA-mRNA network, we calculated the Pearson values and depicted the correlograms through R software. We evaluated the negative correlation between the key miRNA and target expression.

2.5 Reverse transcription quantitative Real-time PCR (RT-qPCR)

We used a gene chip to analyze the gene expression profiles. cDNA fragments were purified with a PCR extraction kit (XXXX) following the manufacturer's instruction and then enriched by RT-PCR. Total RNA was extracted using TRIzol reagent (Life Technologies, USA) and quantified using Thermo Nanodrop 2000. RNA (0.5 μg) was subjected to reverse transcription using the Script cDNA Synthesis Kit (Takara, China). miRNA and mRNA primer sequences are listed in Tables 6 and 7.

2.6 Statistical analysis

Statistical analyses were performed using t test or ANOVA followed by Bonferonni's test, using the GraphPad 6 Prism software (San Diego, CA, USA). Data are expressed as mean ± S.E.M. $P<0.05$ was considered statistically significant.

3. Results

3.1 Differential expression profiles for pediatric AT/RT

Using |fold change|> 2 and *P*-value < 0.01 as a threshold, we identified a total of 581 DEGs in the tumor group compared with the control group. Among the DEGs, 179 were up-regulated and 402 were down-regulated (Table 2, Figure 1A). In addition, 21 differentially expressed miRNAs (DEmiRNAs) were identified, including 5 up-regulated DEmiRNAs and 16 down-regulated DEmiRNAs (Table 3, Figure 1B–C).

3.2 GO enrichment analysis for DEGs

To identify the biological characteristics and signaling pathways involved in the pathogenesis of AT/RT, we next used Clusterprofile in R package to enrich DEGs. The enrichment results of the top 20 genes from the CC, MF and BP categories are shown in Figure 2. The results indicated that many of the DEGs are closely involved in the formation of synapses. Molecular functions analysis indicated that DEGs were involved in binding to specific molecules, such as growth factor binding, calmodulin binding, and activity of passive membrane transporters. The DEGs were also involved in several critical biological progresses including the regulation of synaptic plasticity, modulation of chemical synaptic transmission, and transportation and secretion of the neurotransmitters, which are all involved in the regulation of nervous system plasticity.

3.3 KEGG enrichment analysis for DEGs and the immune infiltration correlation of the expression profile

The KEGG signaling pathway results are shown in Figure 3. DEGs are highly involved in synaptic function and neurotransmitter transmission. The top enriched pathways include the regulation of "Synaptic vesicle cycle," "GABAergic synapse" and "Glutamatergic synapse," which are consistent with the results of GO enrichment, indicating that impaired synaptogenesis and synaptic dysfunction could contribute to the formation and clinical manifestation of AT/RT. DEGs were also shown to modulate the "cAMP signaling pathway," which could affect cell differentiation.

We also analyzed the correlation between the expression profile and immune infiltration pathways to identify the association between immune cell types and AT. The proportions of certain immune cells such as memory T cells, resting dendritic cells, neutrophils, and neutrophils were relatively lower in tumor tissues compared with levels in normal tissues. B cells, activated NK cells, and T follicular helper cells showed no difference between tumor tissues and normal tissues.

3.4 Construction of the AT/RT-associated miRNA-mRNA correlation and network

To clarify the potential roles of significantly dysregulated miRNAs and to further explore miRNA-mRNA regulatory mechanisms in AT/RT, we identified the potential targets of DEmiRNAs and the genes that were inversely co-expressed with DEmiRNAs using the previously shown gene expression profile. The 581 DEmRNAs and 21 mature DEmiRNAs were analyzed using the miRTarBase database (http://mirtarbase.mbc.nctu.edu.tw/). A total of 17 DEmiRNAs were found to negatively regulate at least one of the targets in DEmRNAs. Detailed information for each miRNA-mRNA targeting pair is shown in Table 4. The co-expression network of DEmiRNAs and DEmRNAs was constructed and visualized using Cytoscape software; the results are shown in Figure 4. miR-17a-5p appeared to play the central role in the DEG network; therefore, miR-17A-5p was selected for further analysis.

We next examined the regulatory relationship of miR-17a-5p. The subnetworks shown in Figure 4 revealed the molecular pathways that were altered by miR-17a-5p. There were 15 mRNAs downregulated by miR-17a-5p. In addition, correlation analysis by Pearson coefficient revealed that KIF5C and DPYSL2 had the highest correlation with miR-17a-5p (Figure 4, Table 5).

3.5 Validation of related miRNA expression levels in AT/RT using qRT-PCR

Previous studies have shown that miRNAs play a vital role in tumor progression in AT/RT. We next evaluated the performance of the seven candidate miRNAs (hsa-miR-17-5p, has-miR-18a-5p, hsa-miR-488-5p, hsa-miR-128-3p, hsa-miR-495-3p, hsa-miR-668-3p, hsa-miR-874-3p) in diagnosing AT/RT. qPCR assays demonstrated that higher expression of miR-17-5p and miR-18a-5p in AT/RT compared with normal brain tissues (Figure 5). In addition, the expression of miR-874-3p was lower in AT/RT compared with levels in normal brain tissues.

3.6 Verification for related mRNA expression levels using qRT-PCR

To investigate the potential function and underlying mechanism of miR-17-5p in AT/RT, we used bioinformatics algorithms and mRNA profiling from AT/RT patients to identify potential target genes of miR-17-5p. The binding of a miRNA to its target mRNA can induce translational silencing or degradation, leading to inhibition or enhancement of gene expression. Various studies have performed expression profiling to identify the roles of miRNAs in AT/RT. Our results indicated that MAP7, PRKCB, CDK1,

PPP3R1, CCND1, HDAC1 and CDC20 mRNAs were differentially expressed in AT/RT (Figure 6). It is worth to mention that MAP7 plays an important regulatory role in AT/RT.

Discussion

AT/RT is an aggressive pediatric tumor of the CNS. The limited available treatments and poor prognosis of AT/RT warrants the urgent need to identify novel therapeutic targets and develop innovative treatment strategies for this disease [20, 21]. Mutations and/or deletions of the *SMARCB1* (BAF47/INI1/SNF5) gene are hallmarks of AT/RT tumors, and so far no other recurrent genetic abnormalities have been identified [22]. Previous studies showed that HMGA2, LIN28, RPL5, RPL10 and SUN2 are crucial regulators in AT/RT [23, 24]. However, the precise molecular mechanism of AT/RT remains largely unknown.

miRNAs play crucial roles in regulating gene expression at the transcriptional, post-transcriptional and epigenetic levels. Previous studies have established that miRNAs participate in a wide variety of biological processes including genomic imprinting, cell cycle, cell differentiation, invasion and migration [25, 26]. Hsiehet et al. showed that miR-221/222 represents a promising new target in AT/RT [24]. Our multi-omics analysis identified 5 upregulated miRNAs (hsa-miR-301a-3p, hsa-miR-18a-5p, hsa-miR-335-3p, hsa-miR-18b-5p, hsa-miR-17-5p) and 16 downregulated miRNAs (hsa-miR-129-1-3p, hsa-miR-128-3p, hsa-miR-656-3p, hsa-miR-329-3p, hsa-miR-1224-5p, hsa-miR-668-3p, hsa-miR-488-5p, hsa-miR-29c-5p, etc.) in AT/RT. Hsa-miR-129-1-3p was the most-downregulated in AT/RT while hsa-miR-17-5p was the most up-regulated miRNA in AT/RT.

We further found that 179 mRNAs were up-regulated and 402 mRNAs were down-regulated, which could be the result of the dysregulated miRNA networks in AT/RT, as miRNAs regulate the levels and functions of their target mRNAs. GO analyses revealed that these mRNAs are involved in critical pathways such as the regulation of synaptic plasticity, modulation of chemical synaptic transmission, neurotransmitter transportation and secretion. KEGG pathway analysis showed that “Synaptic vesicle cycle,” “GABAergic synapse” and “Glutamatergic synapse” were related to the DEGs, which is consistent with GO enrichment analysis. These findings suggest that altered synaptogenesis and synaptic dysfunction could contribute to the formation and clinical manifestation of AT/RT. Additionally, DEGs were involved in the canonical pathways such as cAMP signaling pathway, which may contribute to the stemness of the AT/RT tumor cells.

Several recent studies have analyzed the influence of the host immune system on cancer prognosis [27]. We performed analyses using CIBERSORT, a computational method for high-throughput characterization of different types of immune cells in complex tissues. Our results demonstrated there was no difference in immune-related cells in AT/RT.

MiRTarBase database is a database that predict targets for miRNAs [28]. Seventeen DEmiRNAs were found to have at least one negatively regulated miRNA-mRNA pair in the DEmRNAs. Notably, over 30 mRNAs were predicted to be regulated by hsa-miR-17-5p. To further probe the negative correlations

between hsa-miR-17-5p and its target mRNAs, we calculated the Pearson values using R software. A total of 15 mRNAs were negatively correlated with hsa-miR-17-5p. In addition to the protein-protein interaction networks constructed between DEmiRNAs and DEmRNAs, we also further verified the expression of hsa-miR-17-5p, hsa-miR-18a-5p, hsa-miR-488-5p, hsa-miR-128-3p, hsa-miR-495-3p, hsa-miR-668-3p, and hsa-miR-874-3p using qPCR. These results further demonstrated the importance of hsa-miR-17-5p in AT/RT.

Zeng et al previously reported that miRNA-17-5p expression is upregulated in glioblastoma and is a potential marker for the proneural subtype [29]. However, the mechanisms by which miRNA-17-5p expression regulates tumorigenesis are not well elucidated. We screened and identified possible targets of miRNA-17-5p and the results suggested that CCND1, THBS1, WEE1, SIRPA, SOX4, UBE2C, MDK, KIF5C, PTBP1, GPM6A, DPYSL2, PTTG1, TPRG1L, KIAA0513, SCAMP5, RAPGEF4, NRIP3, MAP7, RAB11FIP1, BTG3, MELK, TSPAN6, PEA15, PPP3R1, PGM2L1, LAMC1, IER3, GABBR1, CD47, and ABCA1 genes may play important roles in the pathogenesis of AT/RT. qPCR experiments verified that the expressions of MAP7, CDK1, PPP3R1, PRKC1, CCND1 and HDAC1 genes were indeed altered in AT/RT tumor tissue. Interestingly, *CCND1*, which encodes a crucial regulator of the cell cycle [30], was upregulated in AT/RT. We hypothesize that miRNA-17-5p promotes tumorigenesis in AT/RT by promoting *CCND1* expression and cell cycle entry and progression. In addition, we reported that MAP7 mRNA showed the greatest down-regulation in AT/RT among all identified mRNAs. Together, these studies point to a potential role of miR-17-5p in AT/RT tumorigenesis.

Conclusion

Our findings suggest that the dysregulation of hsa-miR-17-5p may be a pivotal event in AT/RT and MAP7 miRNAs that may represent potential therapeutic targets and diagnostic biomarkers.

Abbreviations

AT/RT: Atypical teratoid/rhabdoid tumor

CNS: Central nervous system

qPCR: Quantitative Real-time PCR

KEEG: Kyoto Encyclopedia of Genes and Genomes

GO: Gene Ontology

BP: Biological process

MF: Molecular function

CC: Cellular component

DEGs: Differentially Expressed Genes

RT-qPCR: Reverse transcription quantitative Real-time PCR

DEmiRNAs: Differentially expressed miRNAs

Declarations

Ethics approval and consent to participate:

Not applicable.

Consent for publication:

Not applicable.

Availability of data and materials:

The authors declare are no conflicts of interest.

Competing interests:

The authors declare are no conflicts of interest.

Funding:

This research was funded by grants from the National Natural Science Foundation Committee of China (No.81572497; 81703011; 81873739; 81372713; 81672497) and the Guangdong Provincial Department of Science and Technology, China (No.2017A030313487).

Authors' contributions:

FCL conceived and designed the study. XKX, HYY, CC, and WC performed the experiments, analyzed the data and wrote the manuscript. YL, HYY, and PJP performed the analysis using bioinformatics. HYY and YL assisted in performing the research, and YL and PJP provided language help and assisted in analyzing data. All authors read and approved the final manuscript.

Acknowledgements:

Not applicable.

References

1. Biegel JA, Zhou J-Y, Rorke LB, Stenstrom C, Wainwright LM, Fogelgren B. Germ-line and acquired mutations of INI1 in atypical teratoid and rhabdoid tumors. Cancer research. 1999;59:74–9.
2. Biswas A, Kashyap L, Kakkar A, Sarkar C, Julka PK. Atypical teratoid/rhabdoid tumors: challenges and search for solutions. Cancer management and research. 2016;8:115.
3. Gigante L, Paganini I, Frontali M, Ciabattoni S, Sangiuolo FC, Papi L. Rhabdoid tumor predisposition syndrome caused by SMARCB1 constitutional deletion: prenatal detection of new case of recurrence in siblings due to gonadal mosaicism. Familial cancer. 2016;15:123–6.
4. Morgenstern DA, Gibson S, Brown T, Sebire NJ, Anderson J. Clinical and pathological features of paediatric malignant rhabdoid tumours. Pediatric blood & cancer. 2010;54:29–34.
5. Paolini MA, Kipp BR, Sukov WR, Jenkins SM, Barr Fritcher EG, Aranda D, et al. Sellar Region Atypical Teratoid/Rhabdoid Tumors in Adults: Clinicopathological Characterization of Five Cases and Review of the Literature. Journal of Neuropathology & Experimental Neurology. 2018;77:1115–21.
6. Wang R-f, Guan W-b, Yan Y, Jiang B, Ma J, Jiang M-w, et al. Atypical teratoid/rhabdoid tumours: clinicopathological characteristics, prognostic factors and outcomes of 22 children from 2010 to 2015 in China. Pathology. 2016;48:555–63.
7. Thatikunta M, Mutchnick I, Elster J, Thompson MP, Huang MA, Spalding AC, et al. Neoadjuvant chemotherapy for atypical teratoid rhabdoid tumors: case report. Journal of Neurosurgery: Pediatrics. 2017;19:546–52.
8. Alimova I, Pierce A, Danis E, Donson A, Birks DK, Griesinger A, et al. Inhibition of MYC attenuates tumor cell self-renewal and promotes senescence in SMARCB1-deficient Group 2 atypical teratoid rhabdoid tumors to suppress tumor growth in vivo. International journal of cancer. 2019;144:1983–95.
9. Hwang H, Mendell J. MicroRNAs in cell proliferation, cell death, and tumorigenesis. British journal of cancer. 2006;94:776.
10. Nana-Sinkam S, Croce C. Clinical applications for microRNAs in cancer. Clinical Pharmacology & Therapeutics. 2013;93:98–104.
11. Ferreira HJ, Esteller M. Non-coding RNAs, epigenetics, and cancer: tying it all together. Cancer and Metastasis Reviews. 2018;37:55–73.
12. Croce CM. Causes and consequences of microRNA dysregulation in cancer. Nature reviews genetics. 2009;10:704.
13. Iorio MV, Croce CM. MicroRNAs in cancer: small molecules with a huge impact. Journal of clinical oncology. 2009;27:5848.
14. Ventura A, Jacks T. MicroRNAs and cancer: short RNAs go a long way. Cell. 2009;136:586–91.

15. Ahir BK, Elias NM, Lakka SS. SPARC overexpression alters microRNA expression profiles involved in tumor progression. Genes & cancer. 2017;8:453.
16. McCarthy DJ, Chen Y, Smyth GK. Differential expression analysis of multifactor RNA-Seq experiments with respect to biological variation. Nucleic acids research. 2012;40:4288–97.
17. Yu G, Wang L-G, Han Y, He Q-Y. clusterProfiler: an R package for comparing biological themes among gene clusters. Omics: a journal of integrative biology. 2012;16:284–7.
18. Newman AM, Liu CL, Green MR, Gentles AJ, Feng W, Xu Y, et al. Robust enumeration of cell subsets from tissue expression profiles. Nature methods. 2015;12:453.
19. Hsu S-D, Lin F-M, Wu W-Y, Liang C, Huang W-C, Chan W-L, et al. miRTarBase: a database curates experimentally validated microRNA–target interactions. Nucleic acids research. 2010;39:D163-D9.
20. Eaton KW, Tooke LS, Wainwright LM, Judkins AR, Biegel JA. Spectrum of SMARCB1/INI1 mutations in familial and sporadic rhabdoid tumors. Pediatric blood & cancer. 2011;56:7–15.
21. Gump JM, Donson AM, Birks DK, Amani VM, Rao KK, Griesinger AM, et al. Identification of targets for rational pharmacological therapy in childhood craniopharyngioma. Acta neuropathologica communications. 2015;3:30.
22. Weingart MF, Roth JJ, Hutt-Cabezas M, Busse TM, Kaur H, Price A, et al. Disrupting LIN28 in atypical teratoid rhabdoid tumors reveals the importance of the mitogen activated protein kinase pathway as a therapeutic target. Oncotarget. 2015;6:3165.
23. Ren Y, Tao C, Wang X, Ju Y. Identification of RPL5 and RPL10 as novel diagnostic biomarkers of Atypical teratoid/rhabdoid tumors. Cancer cell international. 2018;18:190.
24. Hsieh T-H, Chien C-L, Lee Y-H, Lin C-I, Hsieh J-Y, Chao M-E, et al. Downregulation of SUN2, a novel tumor suppressor, mediates miR-221/222-induced malignancy in central nervous system embryonal tumors. Carcinogenesis. 2014;35:2164–74.
25. Sato F, Tsuchiya S, Meltzer SJ, Shimizu K. MicroRNAs and epigenetics. The FEBS journal. 2011;278:1598–609.
26. Kanwal R, Gupta S. Epigenetic modifications in cancer. Clinical genetics. 2012;81:303–11.
27. Schmidt M, Böhm D, Von Törne C, Steiner E, Puhl A, Pilch H, et al. The humoral immune system has a key prognostic impact in node-negative breast cancer. Cancer research. 2008;68:5405–13.
28. Chou C-H, Chang N-W, Shrestha S, Hsu S-D, Lin Y-L, Lee W-H, et al. miRTarBase 2016: updates to the experimentally validated miRNA-target interactions database. Nucleic acids research. 2015;44:D239-D47.
29. Zeng A, Yin J, Wang Z, Zhang C, Li R, Zhang Z, et al. miR-17-5p-CXCL14 axis related transcriptome profile and clinical outcome in diffuse gliomas. Oncoimmunology. 2018;7:e1510277.
30. Gennaro VJ, Stanek TJ, Peck AR, Sun Y, Wang F, Qie S, et al. Control of CCND1 ubiquitylation by the catalytic SAGA subunit USP22 is essential for cell cycle progression through G1 in cancer cells. Proceedings of the National Academy of Sciences. 2018;115:E9298-E307.

Tables

Table 1
Datasets for AT/RT

Datasets	Platform	Description	Controls	Tumors
GSE42656	GPL6947	gene	**8**	**5**
GSE42657	GPL8179	miRNA	**7**	**5**

Table 2
Top 20 DEGs

Gene symbol	logFC	*P*-value	dysregulated
COL3A1	5.009728	2.82E-66	up
CLIC6	4.963553	2.11E-11	up
COL1A1	4.322956	4.55E-14	up
COL1A2	4.049388	5.94E-16	up
COL4A1	4.022476	1.25E-29	up
CTGF	3.988644	6.66E-20	up
ID3	3.752354	3.04E-36	up
TOP2A	3.702338	3.67E-58	up
FSTL1	3.681477	1.07E-31	up
S100A4	3.647612	4.79E-14	up
TF	-5.80568	7.29E-58	down
MBP	-5.63473	1.01E-23	down
PVALB	-5.57699	6.54E-11	down
SNAP25	-5.44596	4.61E-49	down
NDRG2	-5.22185	1.61E-53	down
CAMK2A	-5.22113	2.86E-08	down
EEF1A2	-4.98239	5.91E-41	down
PLP1	-4.89204	9.96E-39	down
FAIM2	-4.79694	2.94E-33	down
SH3GL2	-4.65622	3.74E-23	down

Table 3
DEmiRNAs

miRNA	logFC	*P*-value	dysregulated
hsa-miR-129-1-3p	-4.59055	2.23E-25	down
hsa-miR-128-3p	-4.46518	4.64E-22	down
hsa-miR-656-3p	-3.58948	5.81E-10	down
hsa-miR-329-3p	-3.45779	1.42E-11	down
hsa-miR-1224-5p	-3.22655	1.05E-07	down
hsa-miR-668-3p	-3.13363	3.91E-07	down
hsa-miR-488-5p	-3.11733	1.15E-09	down
hsa-miR-29c-5p	-3.0582	2.44E-10	down
hsa-miR-379-5p	-3.03907	1.70E-07	down
hsa-miR-885-5p	-2.88115	2.84E-05	down
hsa-miR-433-3p	-2.60679	5.77E-05	down
hsa-miR-874-3p	-2.4917	1.26E-07	down
hsa-miR-409-5p	-2.44799	5.69E-06	down
hsa-miR-487b-3p	-2.39918	1.40E-09	down
hsa-miR-495-3p	-2.20978	6.25E-06	down
hsa-miR-889-3p	-2.10228	9.37E-08	down
hsa-miR-301a-3p	2.157525	8.66E-07	up
hsa-miR-18a-5p	2.319174	3.73E-10	up
hsa-miR-335-3p	2.374372	3.30E-06	up
hsa-miR-18b-5p	3.442157	7.63E-10	up

miRNA	logFC	*P*-value	dysregulated
hsa-miR-17-5p	3.53329	7.91E-08	up

Table 4
The co-expression information of DEmiRNAs and DEmRNAs

DEmiRNA	Targets (DEmRNAs)
hsa-miR-1224-5p	CAMK2N1, CLDN1
hsa-miR-128-3p	WEE1, INA, UNC13C, KCNJ6, GAS7, GPR83, TSPAN6, ITPR1, TAGLN, TM4SF1, SOX11, ABCA1, TGFBR3, FAM84B, TPPP, SLC6A17, KBTBD11, GDF15
hsa-miR-129-1-3p	SOX4, SCD5
hsa-miR-17-5p	CCND1, THBS1, WEE1, SIRPA, SOX4, UBE2C, MDK, KIF5C, PTBP1, GPM6A, DPYSL2, PTTG1, TPRG1L, KIAA0513, SCAMP5, RAPGEF4, NRIP3, MAP7, RAB11FIP1, BTG3, MELK, TSPAN6, PEA15, PPP3R1, PGM2L1, LAMC1, IER3, GABBR1, CD47, ABCA1
hsa-miR-18a-5p	IGF2BP2, CTGF, CA12, DAAM2, CDC20, RDH10, CCND1
hsa-miR-18b-5p	CTGF, RDH10, CA12, CCND1
hsa-miR-301a-3p	SERPINE1, NPTX1, SOX4, ATP6V1B2, RAB11FIP1, DPYSL2, MAP7
hsa-miR-329-3p	TIAM1, KCNK1, CTGF, SV2B, KIF5C, MOBP, NECAB1, DAAM2, GPC4, FZD2, NDRG4, SLITRK4, CDK6, STK36, IL1RAPL1, BSN, RIMS3
hsa-miR-335-3p	NECAP1, XKR4, SLC38A1
hsa-miR-379-5p	MICAL2, MICAL2
hsa-miR-433-3p	TYMS
hsa-miR-487b-3p	THBS1
hsa-miR-495-3p	COL4A1
hsa-miR-656-3p	PPP3R1
hsa-miR-668-3p	OSBPL10, CCND1
hsa-miR-874-3p	CNP, HDAC1, NRIP3, MAPT, CAMKV, PEA15
hsa-miR-889-3p	SLC38A1, LOX

Table 5
Correlation Analysis of Target Genes of miR-17a-5p

Gene	r^2	*P*-value
KIF5C	-0.8132933	0.0007215
DPYSL2	-0.7761295	0.001813395
PEA15	-0.7679643	0.002171028
SIRPA	-0.7668815	0.002222304
SCAMP5	-0.7661486	0.002257544
KIAA0513	-0.7638543	0.002370676
MAP7	-0.7522732	0.003010815
CD47	-0.7433326	0.003590814
TPRG1L	-0.7379651	0.003978361
RAPGEF4	-0.7284424	0.004744666
GPM6A	-0.7216386	0.005358348
PPP3R1	-0.6832816	0.010037493
NRIP3	-0.6627694	0.01355686
TSPAN6	0.2707255	0.370982354
ABCA1	0.3972861	0.178873767
WEE1	0.5946464	0.032071943
BTG3	0.6999231	0.007731892
MELK	0.7468654	0.003352146
PTTG1	0.8412606	0.000312887
CCND1	0.8464124	0.0002637
MDK	0.8483379	0.000246983
UBE2C	0.8598805	0.000163567

Table 6
miRNA Primers

Gene	Species	Sequence
hsa-miR-17-5p	*Homo sapiens*	CAAAGTGCTTACAGTGCAGGTAG
hsa-miR-18a-5p	*Homo sapiens*	TAAGGTGCATCTAGTGCAGATAG
hsa-miR-488-5p	*Homo sapiens*	CCCAGATAATGGCACTCTCAA
hsa-miR-128-3p	*Homo sapiens*	TCACAGTGAACCGGTCTCTTT
hsa-miR-495-3p	*Homo sapiens*	AAACAAACATGGTGCACTTCTT
hsa-miR-668-3p	*Homo sapiens*	TGTCACTCGGCTCGGCCCACTAC
hsa-miR-874-3p	*Homo sapiens*	CTGCCCTGGCCCGAGGGACCGA
U6-F	*Homo sapiens*	CTCGCTTCGGCAGCACA
U6-R	*Homo sapiens*	AACGCTTCACGAATTTGCGT
Universal-R	*Homo sapiens*	GCTGTCAACGATACGCTACG

Table 7
mRNA Primers

Gene	Species	Sequences
CCND1	*Homo sapiens*	TGAGGGACGCTTTGTCTGTC
CCND1	*Homo sapiens*	TGAGGGACGCTTTGTCTGTC
CDC20	*Homo sapiens*	AATGTGTGGCCTAGTGCTCC
CDC20	*Homo sapiens*	AGCACACATTCCAGATGCGA
CDK1	*Homo sapiens*	GGCTCTGATTGGCTGCTTTG
CDK1	*Homo sapiens*	ATGGCTACCACTTGACCTGT
PTTG1	*Homo sapiens*	TAACTGGACCAACGGCAACT
PTTG1	*Homo sapiens*	AGAGCTAAACAGCGGAACAGT
PPP3R1	*Homo sapiens*	CGGGTGTTAGGCCAGCTATT
PPP3R1	*Homo sapiens*	AGCTCTTGGCAGTAGCAATGA
CDCA5	*Homo sapiens*	CTGAGCAGTTTGATCTCCTGGT
CDCA5	*Homo sapiens*	CTCAAAGGCAGACAGTCCTCA
PRKCB	*Homo sapiens*	GACCAAACACCCAGGCAAAC
PRKCB	*Homo sapiens*	GATGGCGGGTGAAAAATCGG
HDAC1	*Homo sapiens*	TGCTAAAGTATCACCAGAGGGT
HDAC1	*Homo sapiens*	GGAGCGGGTAGTTAACAGCA
MAP7	*Homo sapiens*	TGCCAAGTGGCTGGTACTAT
MAP7	*Homo sapiens*	GGAATTGGCCTTGCATTGGT
DPYSL2	*Homo sapiens*	AGATCCAACTTTGCCGCTT
DPYSL2	*Homo sapiens*	CGTCTGCCAGTCCCTAAGT
CD47	*Homo sapiens*	ACCTCCTAGGAATAACTGAAGTG
CD47	*Homo sapiens*	GGGTCTCATAGGTGACAACCA
GAPDH	*Homo sapiens*	AACGGATTTGGTCGTATTGGG
GAPDH	*Homo sapiens*	CCTGGAAGATGGTGATGGGAT

Figures

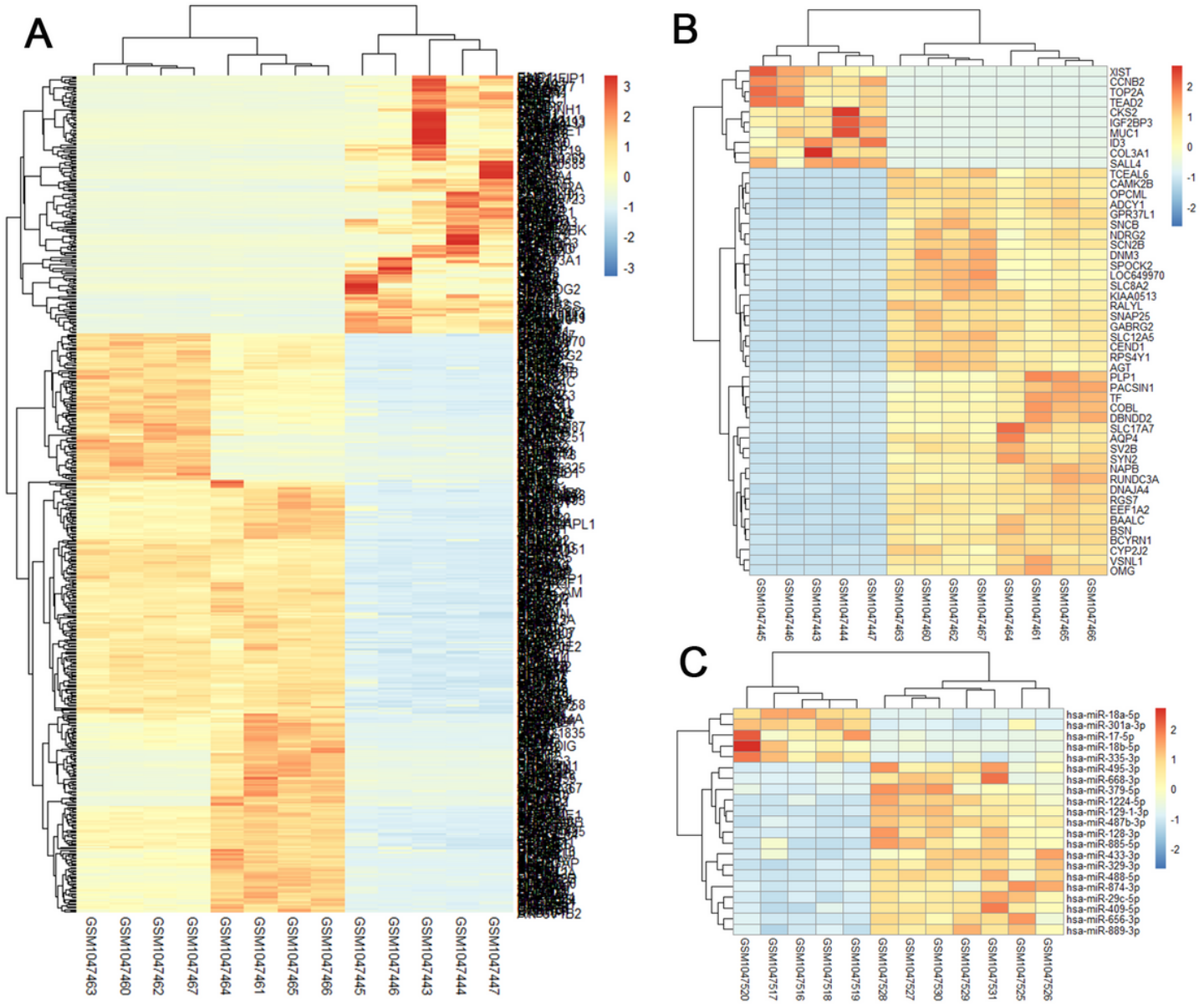

Figure 1

Differential gene expression analysis of pediatric atypical teratoid tumors. A: Heat map depicting gene expression from 13 AT/RT cases and normal brain (columns; ordered automatically by hierarchical clustering). A gradient 'heat spectrum' appears at the right; red indicates increased expression, whereas blue denotes decreased levels. B: Heat map illustrating the expression of 50 mRNAs. C: Heat map illustrating the expression of 21 differentially expressed miRNAs (fold change> 2 and P-value < 0.01).

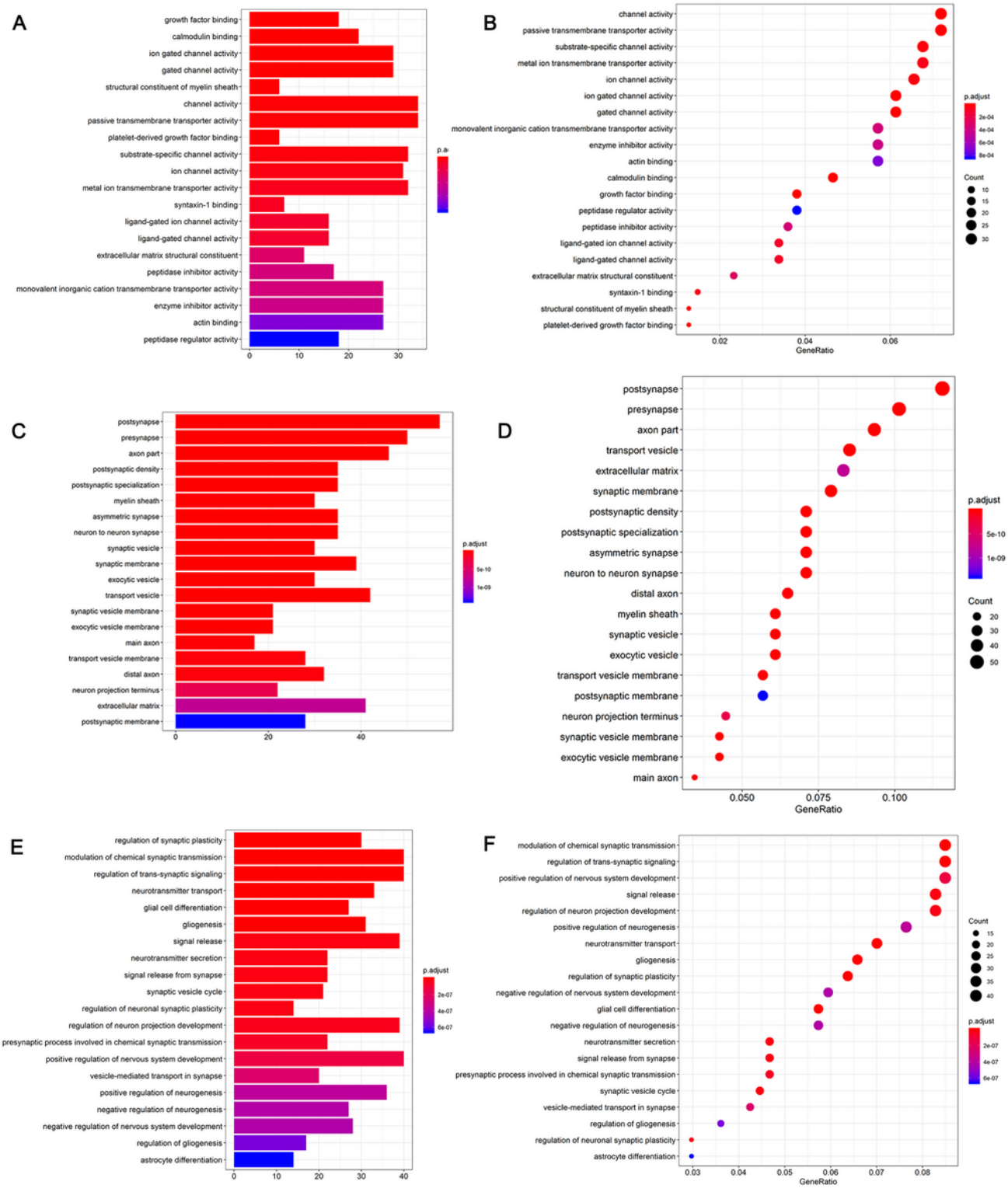

Figure 2

GO enrichment analysis for DEGs in pediatric atypical teratoid tumors. A, C, E: Barplots show the top 20 enrichment terms of CC, MF, and BP, respectively. Each bar represents a term, and the length represents the number of genes enriched. B, D, F: Dotplots represent the top 20 enrichment results of CC, MF, and BP, respectively. The size of each point represents the number of genes enriched; the color represents the degree of enrichment.

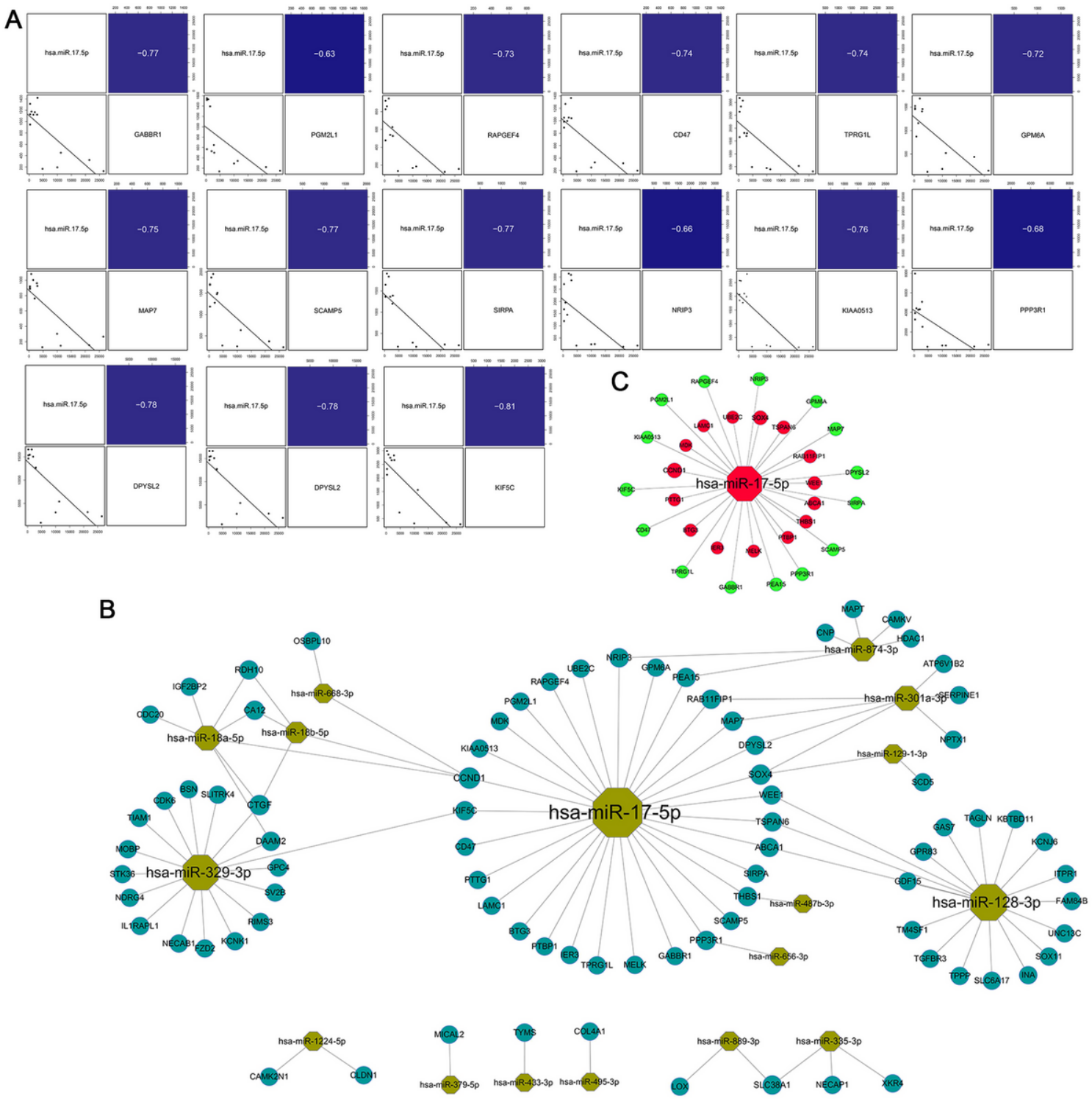

Figure 3

KEGG enrichment analysis for DEGs and the immune infiltration correlation of the expression profile in pediatric AT/RT. A: Barplot shows the top 20 enrichment results from KEGG. The length represents the number of genes enriched. B: Dotplot presents the top 20 enrichment results from KEGG. The size of each point represents the number of genes enriched. C: Bar charts summarize immune cell subset proportions against AT/RT p-value by study

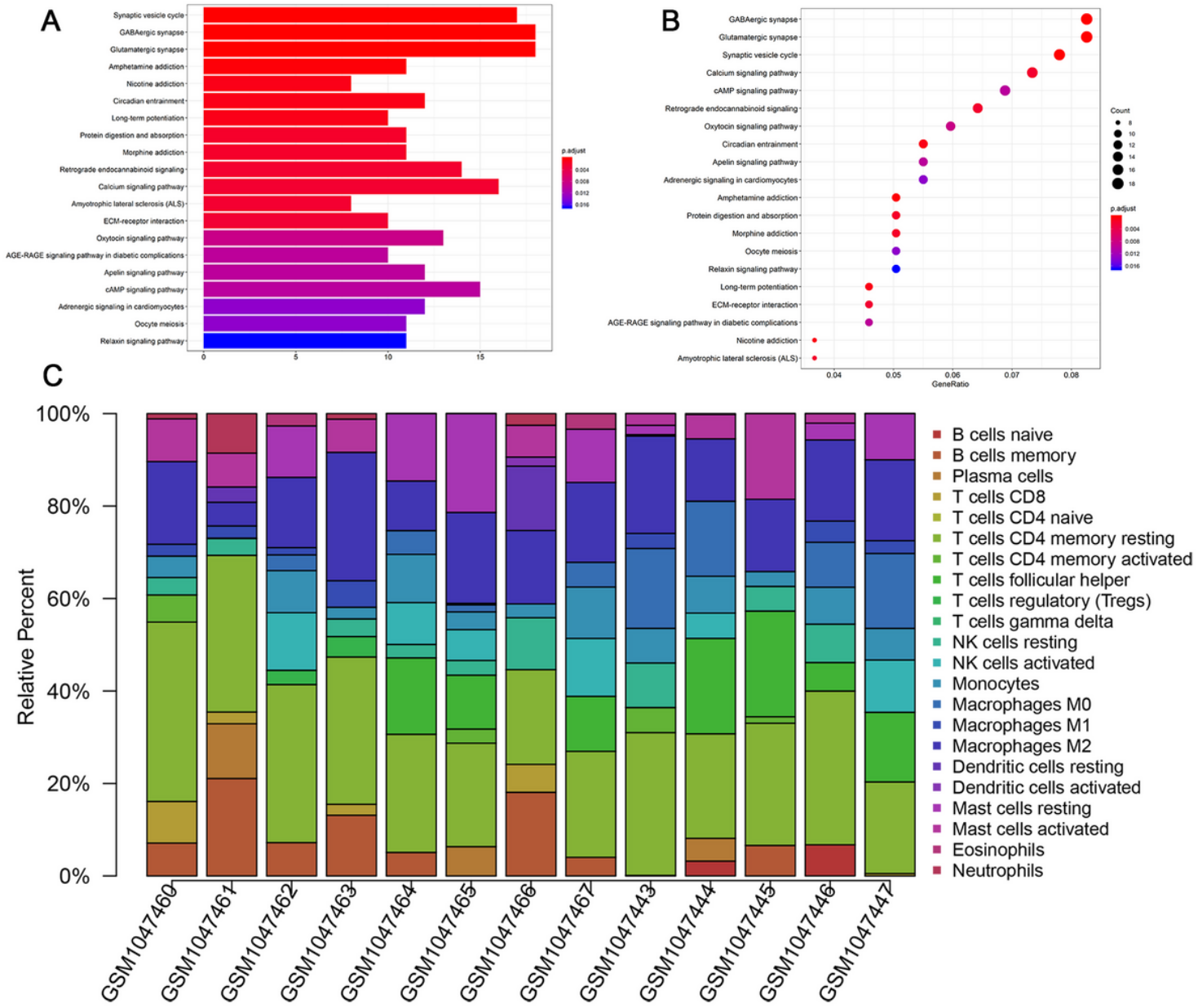

Figure 4

Correlation analysis and network of AT/RT-associated miRNA-mRNA. A: The correlation analysis of miR-17A-5p and 15 downregulated mRNAs by Pearson coefficient. B: The subnetworks revealed the molecular pathways that were altered by miR-17a-5p. C: The co-expression network of differentially expressed miRNAs and mRNAs was constructed.

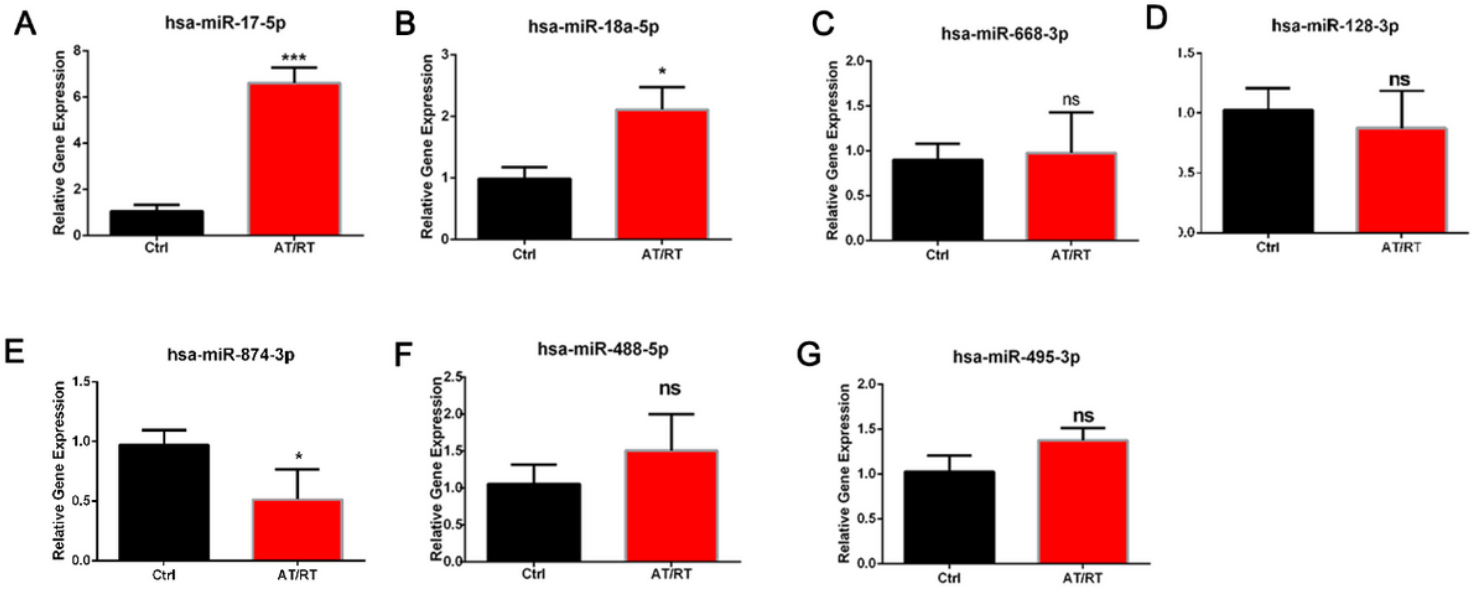

Figure 5

The related miRNA expression level using quantitative real-time PCR in AT/RT. A–G: The relative expression levels of hsa-miR-17-5p, has-miR-18a-5p, hsa-miR-488-5p, hsa-miR-128-3p, hsa-miR-495-3p, hsa-miR-668-3p, and hsa-miR-874-3p (*P<0.05, compared with control; **P<0.01, compared with control; ***P<0.001 compared with control).

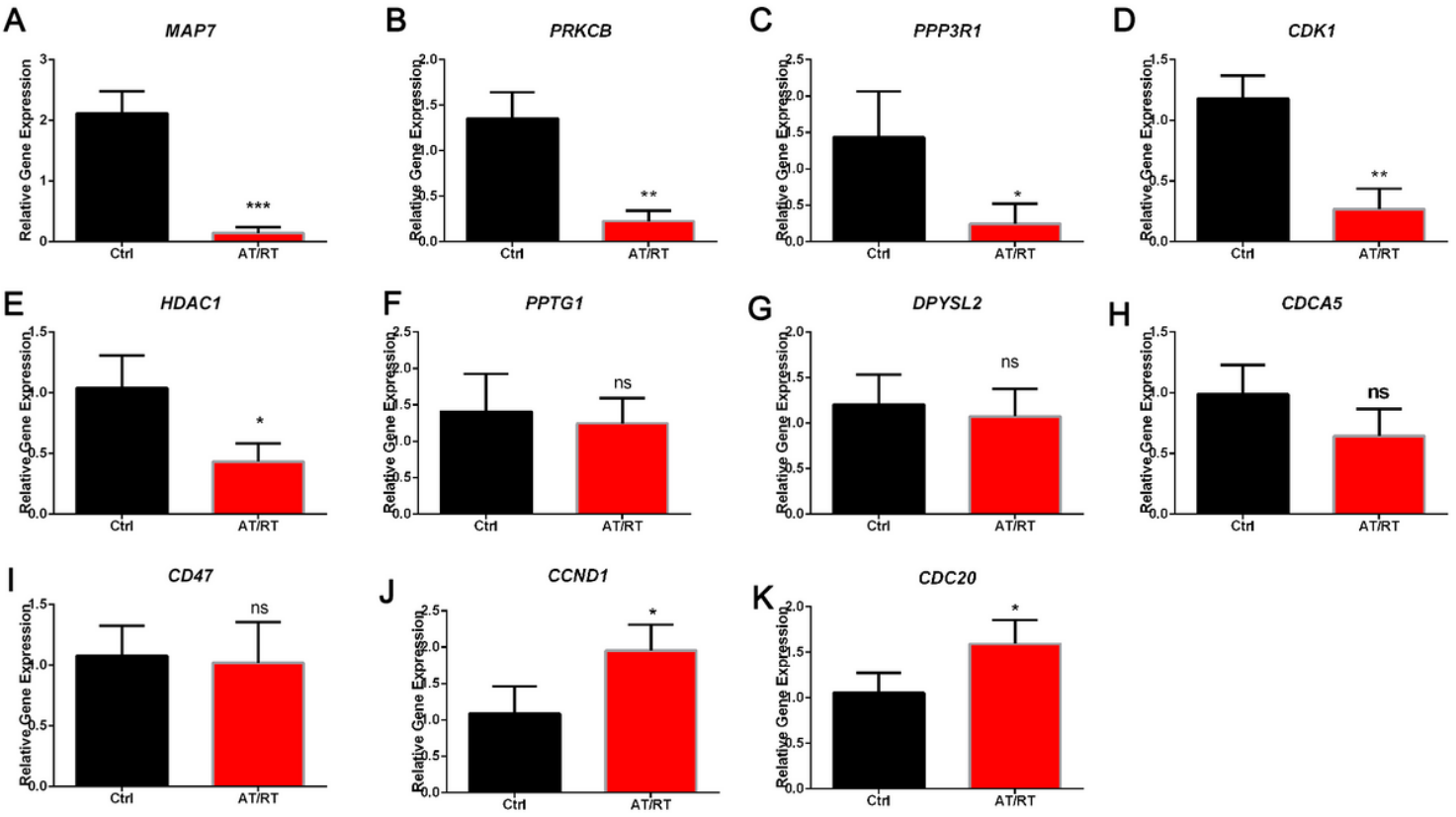

Figure 6

Quantitative real-time PCR of related mRNAs in AT/RT. A–K: The relative expression levels of MAP7, PRKCB, PPP3R1, CDK1, HDAC1, PPTG1, DPYSL2, CDCA5, CD47, CCND1 and CDC20 mRNAs (*P<0.05, compared with control; **P<0.01, compared with control; ***P<0.001 compared with control).